Electric supporting information

A "1-methylimidazole-fixation" route to anchor the small-sized nitrides on carbon supports as non-Pt catalyst for hydrogen evolution reaction

Meichen Meng, Haijing Yan, Yanqing Jiao, Aiping Wu, Xiaomeng Zhang, Ruihong Wang and Chungui Tian*

Key Laboratory of Functional Inorganic Material Chemistry, Ministry of Education of the People's Republic of China, Heilongjiang University, Harbin 150080
E-mail:Chunguitianhq@163.com

The contents of ESI

MD.

12. **Figure S12.** a) Polarization curves of the Pt/C catalysts in 0.5 M H_2SO_4 at a scan rate of 5 mV s^{-1} was obtained by RDE rotated at 1,600 rpm. b) Tafel slopes of the Pt/C catalysts. It shows that the Pt/C given a remarkable HER activity with onset potential close to 0 mV and Tafel slopes 30mV/decade.
13. **Figure S13.** The curves of exchange current density of CNTs, WN/CNTs-50, Mo_2N/CNTs-50 and WN-Mo_2N/CNTs-50.
14. **Figure S14.** CVs for WN-Mo_2N/CNTs-50 with different rates from 20 to 200 mV s^{-1}. The inset is the capacitive currents at 0.39 V as a function of scan rate for WN-Mo_2N/CNTs ($\Delta j_0 = j_a - j_c$). The capacitance of WN-Mo_2N/CNTs-50 is 44 mF cm^{-2}.
15. **Figure S15.** CVs for Mo_2N /CNTs-50 with different rates from 20 to 200 mV s^{-1}. The inset is the capacitive currents at 0.39 V as a function of scan rate for Mo_2N /CNTs-50 ($\Delta j_0 = j_a - j_c$). The capacitance of Mo_2N /CNTs-50 is 32 mF cm^{-2}.
16. **Figure S16.** CVs for WN/CNTs-50 with different rates from 20 to 200 mV s^{-1}. The inset is the capacitive currents at 0.39 V as a function of scan rate for WN/CNTs-50 ($\Delta j_0 = j_a - j_c$). The capacitance of WN/CNTs-50 is 14.3 mF cm^{-2}.
17. **Figure S17.** the W4f spectra of WN/CNTs-50 and WN-Mo_2N/CNTs-50.
18. **Figure S18.** the Mo3d spectra of Mo_2N/CNTs-50 and WN-Mo_2N/CNTs-50.
19. **Figure S19.** a) XRD and b) Large-scale TEM and c) large-magnification TEM image of Mo_2N/CB-50.
20. **Figure S20.** TEM images of WN/rGO-50.
21. **Scheme S1.** the mode of binding of 1-MD to POMs.
22. **Scheme S2.** the mode of binding of 1-MD to CNTs.
23. **Table S1.** the summary of electrochemical performance of different catalysts.

Experimental Section

Chemicals

1-methylimidazole (1-MD), phosphotungstic acid hydrate ($H_3O_{40}PW_{12}.xH_2O$), Phosphomolybdic acid hydrate ($H_3Mo_{12}O_{40}P$) were purchased from Aladdin Chemical Reagent Co., Ltd. The ethanol was purchased from Tianjin Kermel Chemical Reagent Co., Ltd. All regents were used without further treatment. The hydroxylating CNTs were purchased from Shenzhen Nanotech Port Co., Ltd.

Acidification of carbon nanotubes

Hydroxylating carbon nanotubes (5 g), HNO_3 (65%, 50 mL), H_2SO_4 (98%, 150 mL) were added into a 500 mL beaker. The beaker was immersed in a thermostatic water bath (60℃) with vigorous agitation for 30 min. The dispersion was treated under the ultrasonication (60℃) for 30 min to make reaction more adequately. The process was performed for 5h. After cooling to room temperature, the mixture was diluted with 1000 mL deionized water and then vacuum filtered. The filter cake was dispersed in 200 mL of water and filtered again. The washing steps were repeated for several times until the pH of the filtrate reached to 7. The final solid was washed with ethanol and dried under vacuum for 24 h at 60 ℃. The sample was denoted as Acid-CNTs (A-CNTs).

Preparation of WN/CNTs by 1-methylimidazole-fixation" route

A-CNTs (0.1 g) were dispersed in anhydrous ethanol (50 mL) to form a uniform suspension. To realize effective anchoring of POM on CNTs, the pre-modification of CNTs with 1-MD was preformed. After that, 0.5 mL of 1-MD was added into above dispersion. After stirring for 2h at 25^{o}C, the solids were separated by filtration and 1-MD modified CNTs was obtained (1-MD/CNTs). The solids were dispersed into anhydrous ethanol (50 mL) under ultrasound. Then, 0.1g of PW_{12} dissolved into 20 mL of anhydrous ethanol was added into above dispersion. In this step, a pat of PW_{12} can be anchored onto 1-MD-CNTs by 1-MD to provide nuclei sites. After thorough ultrasound, 0.5 mL of 1-MD in 20 mL ethanol was added into the suspension under stirring. The stirring was processed for 10h at least at room temperture. The vacuum

filtration was used to separate the solid, and the PW_{12}/CNTS was obtained after vacuum drying for 1 hour at 60 ℃ (For the clarification, the 1-MD was omitted). PW_{12}/CNTs were calcined at 220 ℃ for 3 h in the air atmosphere and then nitriding in the NH_3 atmosphere at 700 ℃ for 3h. The final product was named WN/CNTs-50. The 50 represent the theoretical amount of POMs in POMs/CNTs, about 50% in this preparation. The WN/CNTs-30, WN/CNTs-70 was prepared by same process except the use of different amount of PW_{12}. The Mo_2N/CNTs-50, Mo_2N/CB-50 and WN/rGO-50 can be synthesized by rationally changing the PW_{12} to PMo_{12}, or replacement of CNTs with carbon black. Different with CNTs, the GO and CB do not need the treatment with acids.

Characterizations

A Bruker D8 Focus Powder X-ray diffractometer was used to characterize samples using Cu Kα radiation (λ=1.5406 Å). Transmission electron microscopy (TEM: JEM-2100) was operated at an accelerating voltage of 200 kV. Raman measurement was taken using a Jobin Yvon HR 800 micro-Raman spectrometer at 457.9 nm. Fourier transform infrared spectrum (FTIR) was obtained from a NICOLETiS10 spectrometer. X-ray photoelectron spectroscopy was implemented on a VG ESCALABMK II apparatus with a Mg K_{α} achromatic X-ray source (1253.6 eV).

Electrochemical measurement

Electrochemical measurements were performed on a BAS100B electrochemical workstation. All the electrochemical tests were carried out in 0.5 M H_2SO_4 electrolyte using a conventional three-electrode at room temperature. Saturated calomel electrode and platinum wire were served as reference and counter electrodes. A rotating disk electrode (RDE) of 3.0 mm in diameter was used as the working electrodes. 5 mg of the catalysts were dispersed in 1 mL mixture solution included 40 μL Nafion solution and water/ethanol (v/v=3:1) solution. After ultrasonication, 10 μL of the catalyst ink was drop-casted onto the GCE with catalyst loading 0.7077 mg cm^{-2}. Linear sweep voltammograms were tested at a scan rate of 5 mV s^{-1}, while RDE was rotated at 1,600 rpm. Long-term stability tests were performed for 12 h. The CV measurements

were performed with different scan rates from 20 to 200 mV s^{-1}. The double-layer capacitor was used to calculate ECSA of catalysts on RDE at 0.39 V. All the potentiometrics were calibrated against the reversible hydrogen electrode (RHE).

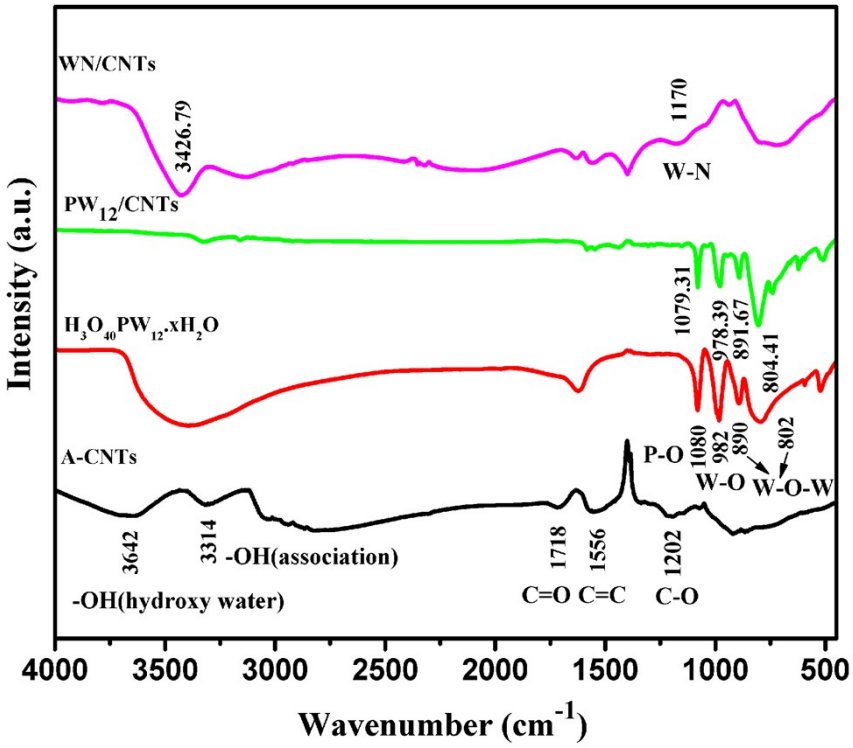

Figure S1. IR spectra of the samples from different step in the preparation of WN/CNTs-50.

In infrared spectrum of acidifying carbon nanotubes, the peaks of intra-molecular association O-H (3314 cm^{-1}), C=O (1718 cm^{-1}), C=C (1556 cm^{-1}), C-O (1202 cm^{-1}) were emerged. For PW_{12}, we can distinctly find that four outstanding characteristic absorption peak situated at 1080 cm^{-1} (P-O), 982 cm^{-1} (W-O), 890 cm^{-1} (W-O-W), 802 cm^{-1} (W-O-W). These intensive peaks also can be observed in the samples of PW_{12}/CNTs, which demonstrate the existence of basic framework of PW_{12} in the samples. However, after the treatment with NH_3, no obvious characteristic peaks of POM were observed. The peaks located at 1170 cm^{-1} can be ascribed to W-N bond. The analysis shows that the conversion of W-O to W-N is achieved and the WN/CNTS complex is formed.

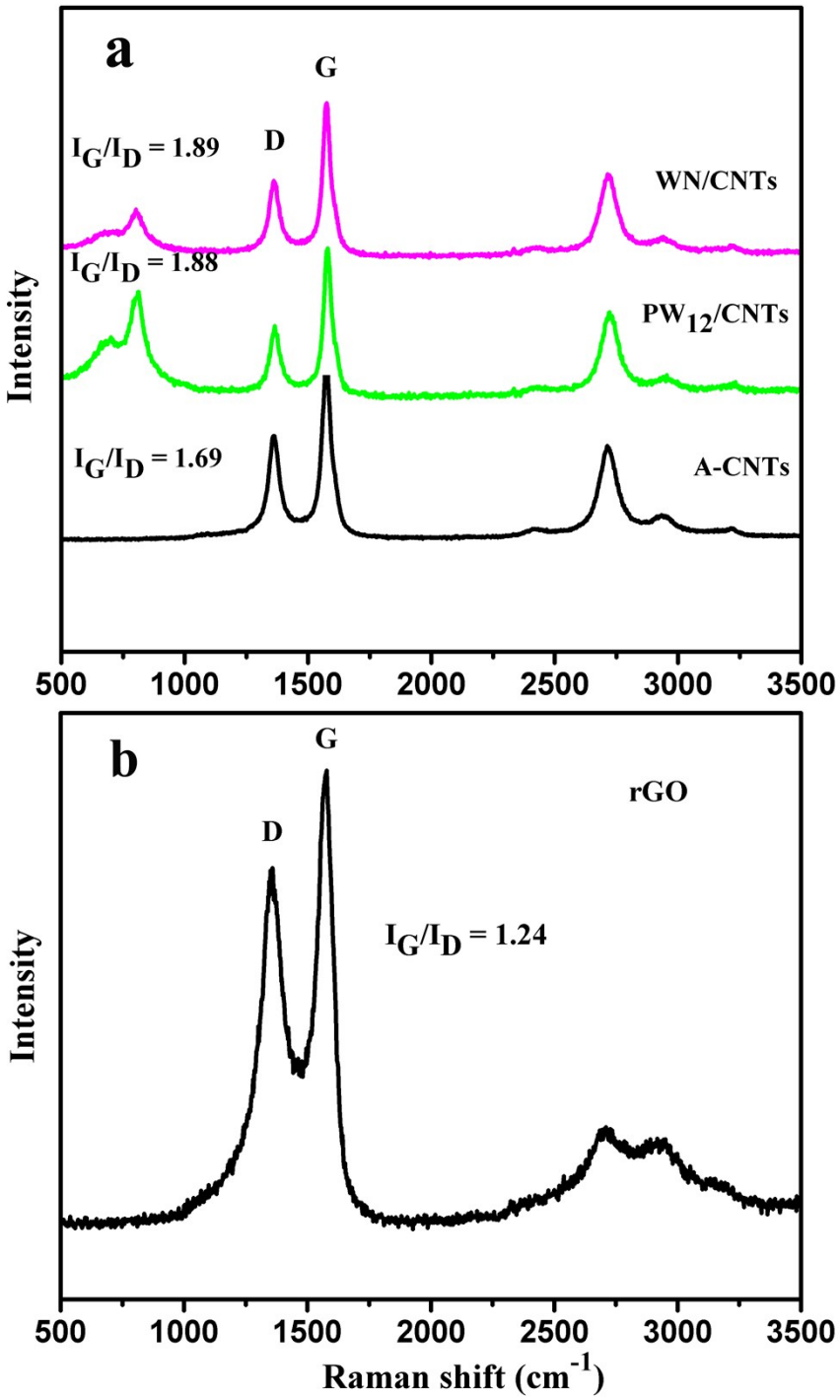

Figure S2. Raman spectra of the samples from a) different step in the preparation of WN/CNTs and b) rGO.

In the Raman spectra, we can observe the two prominent peaks located at 1360 cm^{-1} and 1575 cm^{-1}, which respectively belong to D band and G band of CNTs. The intensity ratio of G band to D band (I_G/I_D) is used to measure the order of carbon materials as a rule. The higher specific value represents that carbon materials verge on

perfect crystals, which have superior crystallinity. It can be seen that all samples shows high ratio of I_G/I_D, demonstated the good crystallinity of the samples. The I_G/I_D ratio of PW_{12}/CNTs, WN/CNTs and A-CNTs are 1.88, 1.89 and 1.69, respectively. In the meantime, the values are higher than 1.24 of reduced Graphene Oxide (rGO, **Figure S2b**) derived from GO, implying the better crystallinity of A-CNTs than rGO. Compared with CNTS, the new small peak located at around 800 cm^{-1} appeared in the other two samples containing W. For the samples of PW_{12}/ CNTS, the vibrational peak situated at 803 cm^{-1} was assigned to stretching vibration of W-O band. The vibration peak at 807 cm^{-1} can be ascribed to the W-N band, which indicated the formation of WN/CNTs. Raman results indicated the trasformation form PW_{12}/CNTs to WN/CNTs, being consistant with that of XRD.

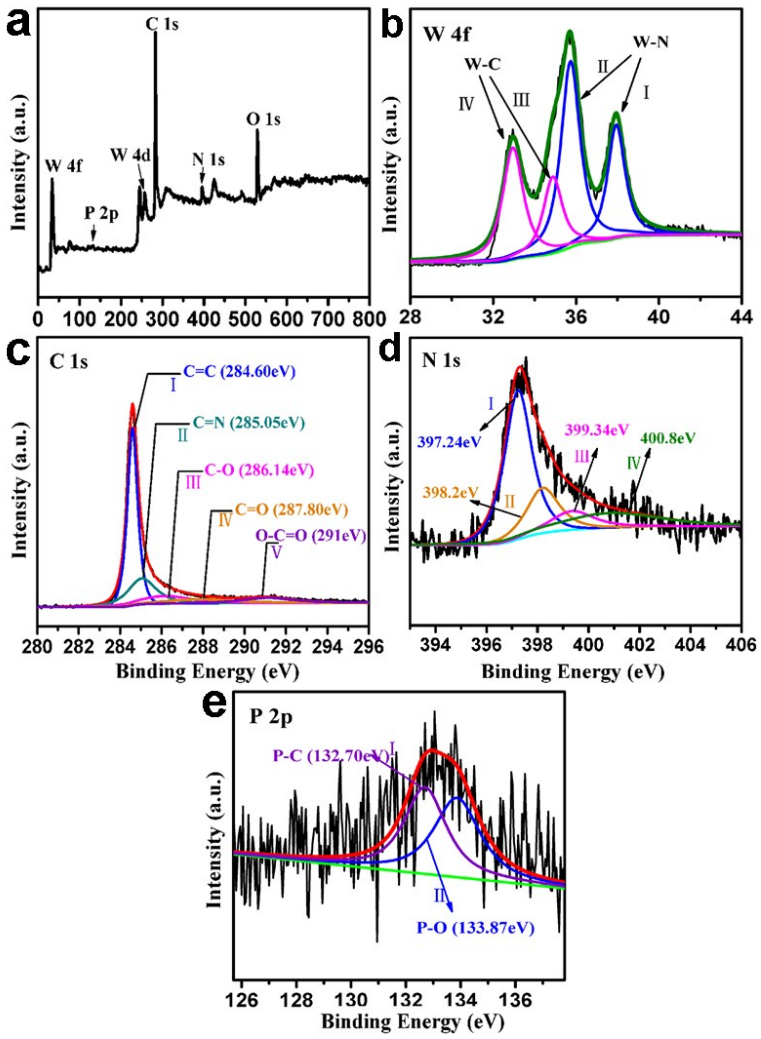

Figure S3. XPS spectra of WN/CNTs-50: a) the survey spectrum, and the high

resolution XPS spectra of b) W4f, c) C 1s, d) N1s and e) P2p.

The elements and valence of WN/CNTs-50 are characterization by XPS. The survey spectrum shows the presence of C (about 285 eV), N (about 398 eV) and O (about 531 eV), P (about 133 eV) and W (about 34 eV) elements in the sample (Figure S3a). The W4f of WN/CNTs samples can be deconvoluted into two sub-groups. The peaks located at about 35.7eV and 37.9eV can be ascribed into W-N, and those located at 32.9 and 34.9 eV is due to presence of W-C. The presence of W-C should be due the reduction role of carbon-containing species under heating.

The C1s spectrum of WN/CNTs-50 sample can be deconvoluted into five sub-peaks labeled with I, II, III, IV and V, Peak I represents graphitic carbon with C–C, C=C and C–H bonds at a BE of 284.6 eV. The peaks located at higher binding energy indicate the existence of carbon combined with nitrogen and oxygen groups. Specifically, Peak II located at 285.05 eV is ascribed to the carbon in C–N bonds. The formation of C–N bonds should be attributed to the reaction of NH_3 with the carbon in CNTs. The peaks III, IV and V can be indexed to the carbon from C–O bonds (286.1 eV), C=O bonds (287.8 eV) and carboxyl groups (O=C–O) (291 eV), respectively. In addition, the high-resolution XPS spectrum shows the presence of the four types of N-containing groups (Figure S3c, d). Peak I located at 397.2 eV is ascribed to N in W-N. Other peaks located at 398.2eV, 399.3eV and 400.8eV can be ascribed to the pyridinic-N (N-2), pyridine-N (N-3), quaternary-N (N-4,). The N are formed through substituting one carbon atom with N on edges or defect sites in the CNTs. The XPS spectrum of P2p can be deconvoluted in two peaks located at 132.7 and 133.87 eV, which can be ascribed to P-C and P-O bonding [Ref. 1], respectively. (Figure S3e)

Ref. 1 H. J. Yan, C. G. Tian, L. Wang, A. P. Wu, M. C. Meng, L. Zhao, and H. G. Fu, *Angew. Chem. Int. Ed.*, 2015, **54**, 6325-6329.

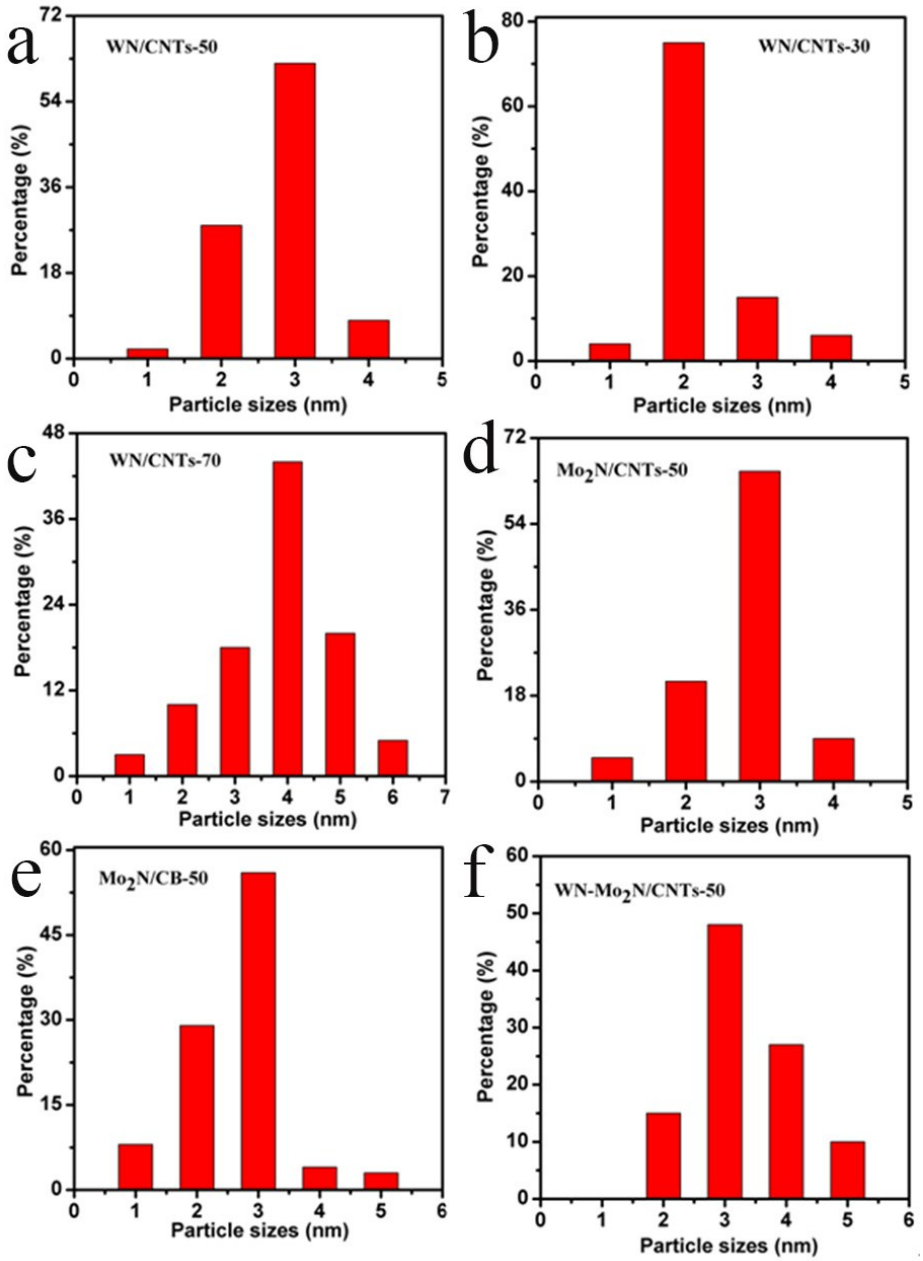

Figure S4. the size distribution histogram of a) WN/CNTs-50, b) WN/CNTs-30, c) WN/CNTs-70, d) Mo_2N/CNTs-50, e) Mo_2N/CB-50 and f) WN-Mo_2N/CNTs-50.

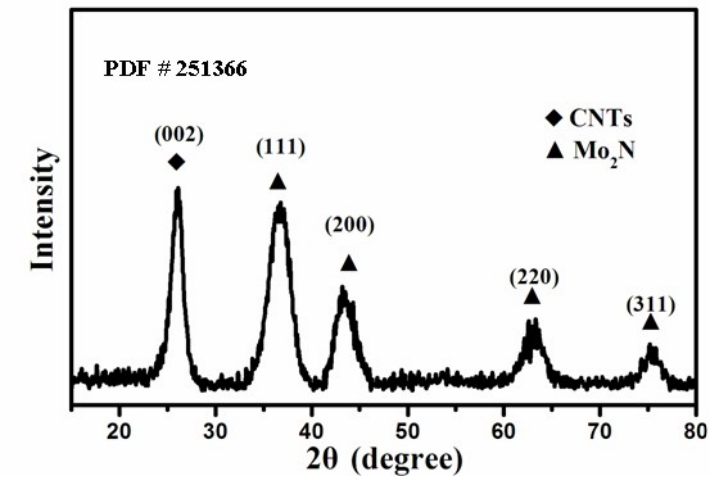

Figure S5. XRD of Mo_2N/CNTs-50 sample.

In XRD spectrum, the peak located at about 26.1° was characteristic for (002) crystal plane of CNTs (Figure S5). Four distinct diffraction peaks located at 37.3°, 43.4°, 63.1°,75.7° are separately referred to (111), (200), (220) and (311) diffraction of primitive cubic structured Mo_2N. No other diffraction peaks are detected in XRD pattern.

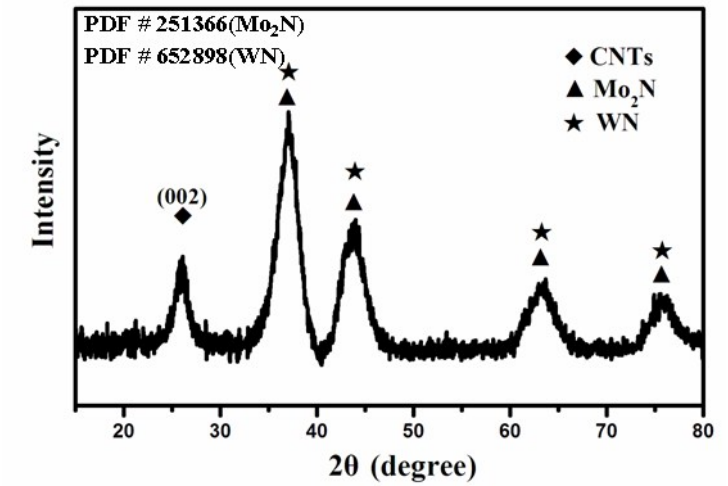

Figure S6. XRD of WN-Mo_2N/CNTs-50

In XRD spectrum, the peak located at about 26.1° was characteristic for (002) crystal plane of CNTs (Figure S6). Four distinct diffraction peaks located at 37.4°, 43.8°, 63.5°, 76° can be observed. It is difficult to distinguish the diffractions of WN and Mo_2N due to their similar position. Howerer, it is found that the peaks is in the between of (111), (200), (220) and (311) diffraction of primitive cubic Mo_2N and fcc structured WN. No other diffraction peaks can be seen obviously in XRD pattern. The

results imply the formation of WN and Mo_2N phase in the WN-Mo_2N/CNTs-50. The presence of W, Mo in the samples was demonstrated by XPS spectra below.

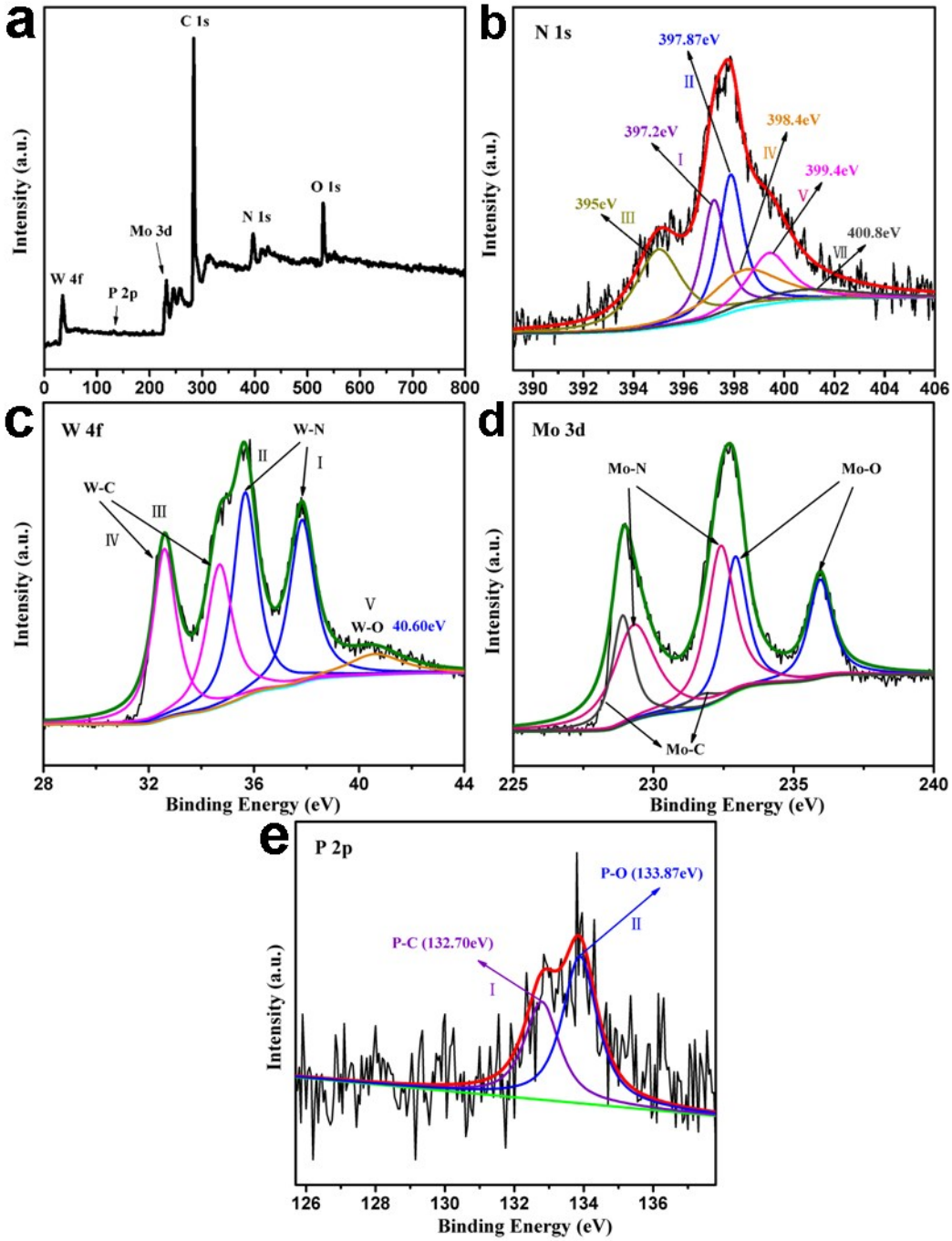

Figure S7. XPS of WN-Mo_2N/CNTs-50. a) the survey spectrum, and the high resolution XPS spectra of b) N1s, c) W4f, d) Mo3d, e) N1s and e) P2p.

The elements and valence of WN-Mo_2N/CNTs-50 are detected by XPS. The survey spectrum shows the presence of C (about 285 eV), N (about 398 eV) and O (about 531 eV), P and W and Mo elements in the sample (Figure S7a). The high-

resolution XPS spectrum shows the presence of the six types of N-containing groups (Figure S7b). The Peak located at 397.9 eV is ascribed to N in W-N, and that located at 397.2eV is ascribed to N in Mo-N. Other peaks located at 398.4eV, 399.4eV and 400.8eV can be ascribed to the pyridinic-N, pyridine-N and quaternary-N. In addition, one peak located at 395eV corresponds to the $Mo3p_{3/2}$. For W4f of WN-Mo_2N/CNTs, after the deconvolution, the W combined with N can be observed at about 35.6 and 37.8 eV. At the same time, the peaks relative with W-C located at 32.7 and 34.7 eV. For the sample, a small peaks of W-O also emerged. For Mo3d of WN-Mo_2N/CNTs, after the deconvolution, the peaks of Mo-N, Mo-O and Mo-C can also be observed. The Mo-N peaks located at 229.3 and 223.4eV.

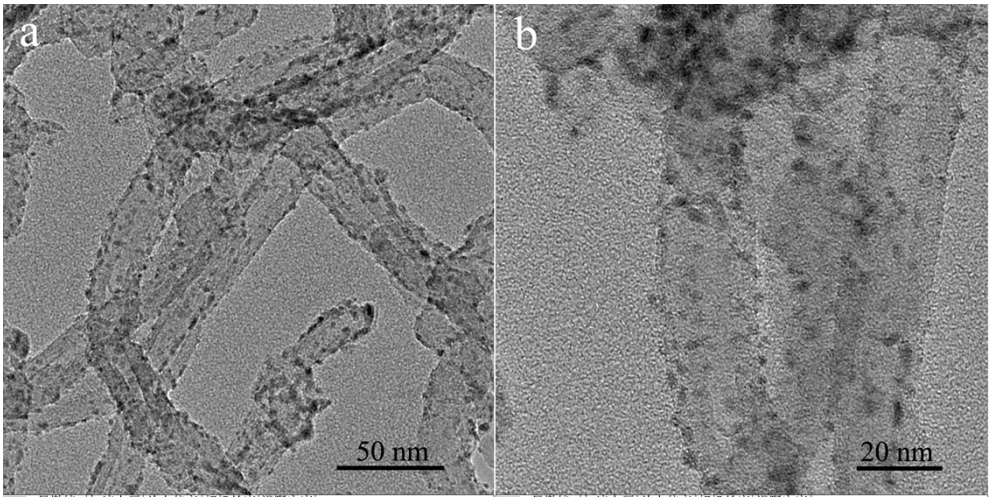

Figure S8. TEM images of WN-Mo_2N/CNTs-50

Figure S8 displays the TEM images of WN-Mo_2N/CNTs-50. We can see that the small particles are uniformly loaded on CNTs (Figure S8a). The size of the particles is about 3 nm (Figure S4f). **The combination of XRD, XPS and TEM indicates the WN and Mo_2N with small size can be ahchored on CNTs by the present method.**

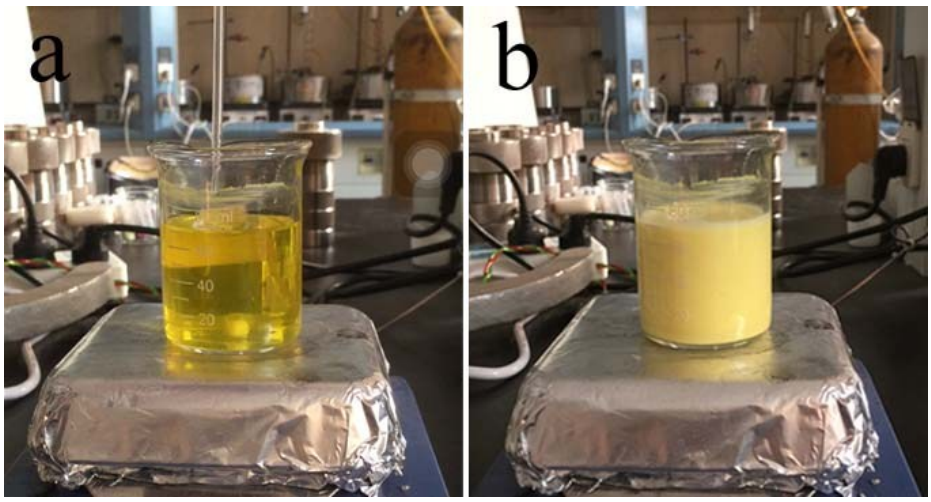

Figure S9. The digital photos of PMo_{12} in ethanol a) before and b) after add of 1-MD.

We can see that the PMo_{12} can be well dissolved in ethanol to form a clear solution. After adding the 1-MD, a yellow precipitation is formed rapidly. The result indicates the effective combination of PMo_{12} with 1-MD, which should be important for anchoring the PMo_{12} onto carbon supports by 1-MD.

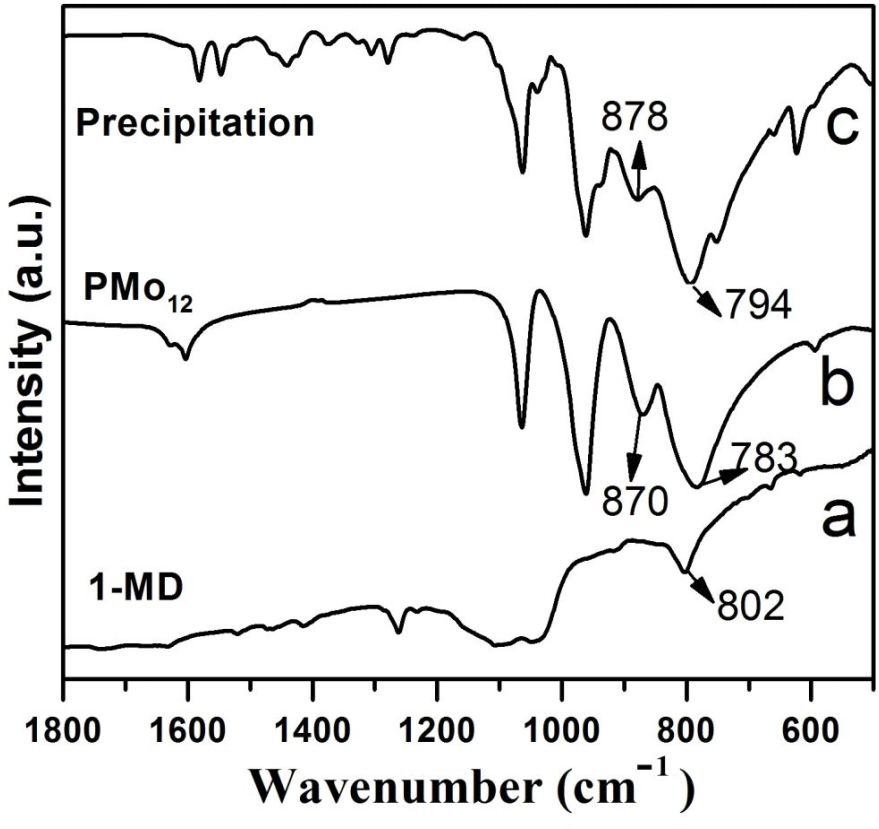

Figure S10. The IR spectra of 1-MD, PMo_{12} and precipitation formed after adding 1-MD in ethanol solution of PMo_{12}.

Figure S10 give the IR spectra of 1-MD, PMo_{12} and precipitation formed after

adding 1-MD in ethanol solution of PMo_{12}. We can see that the IR spectrum of precipitation shows both the peaks from 1-MD and PMo_{12}, indicating the presence (combination) of 1-MD and PMo_{12} units in the precipitation. Also, we can see the peak located at 870 cm^{-1} for PMo_{12} have been shifted to 878cm^{-1} for the precipitation, implying presence of some interaction between 1-MD and PMo_{12}.

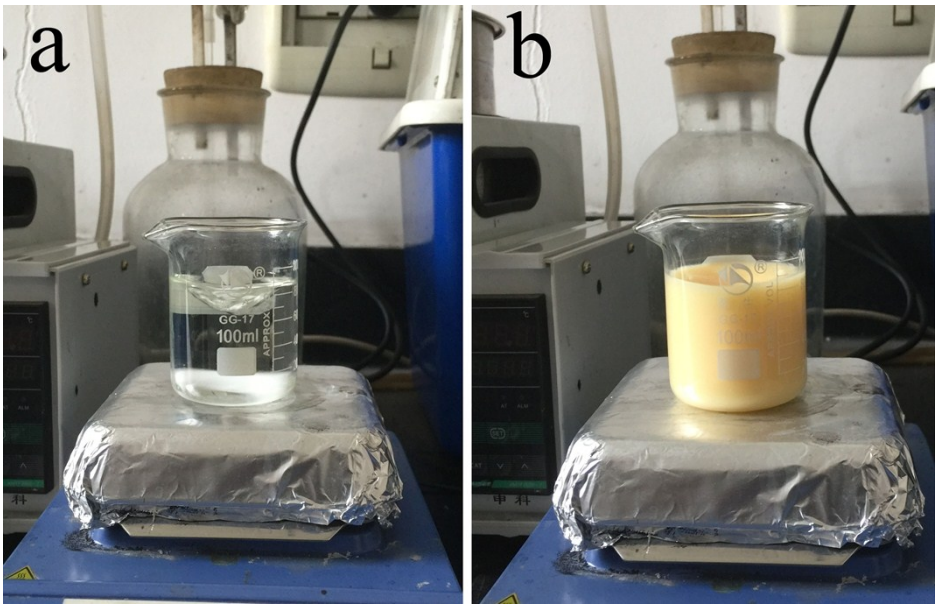

Figure S11. The digital photos of PW_{12} in ethanol a) before and b) after add of 1-MD.

The PW_{12} can be well dissolved in ethanol to form a clear and colorless solution. After adding 1-MD into the solution, a precipitation is formed rapidly. The result indicates the effective combination of PW_{12} with 1-MD, which should be important for anchoring the PW_{12} onto carbon supports by 1-MD.

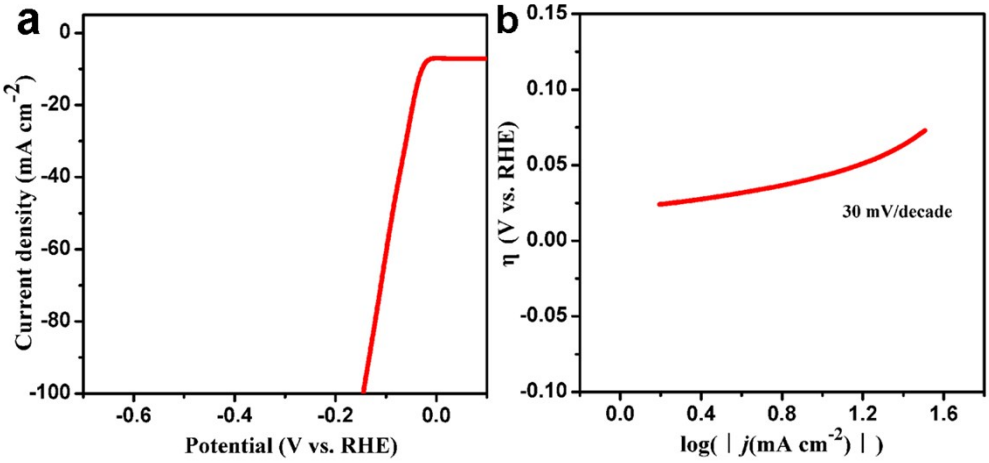

Figure S12. a) Polarization curves of the Pt/C catalysts in 0.5 M H_2SO_4 at a scan rate of 5 mV s^{-1} was obtained by RDE rotated at 1,600 rpm. b) Tafel slopes of the Pt/C catalysts. It shows that the Pt/C given a remarkable HER activity with onset potential close to 0 mV and Tafel slopes 30mV/decade.

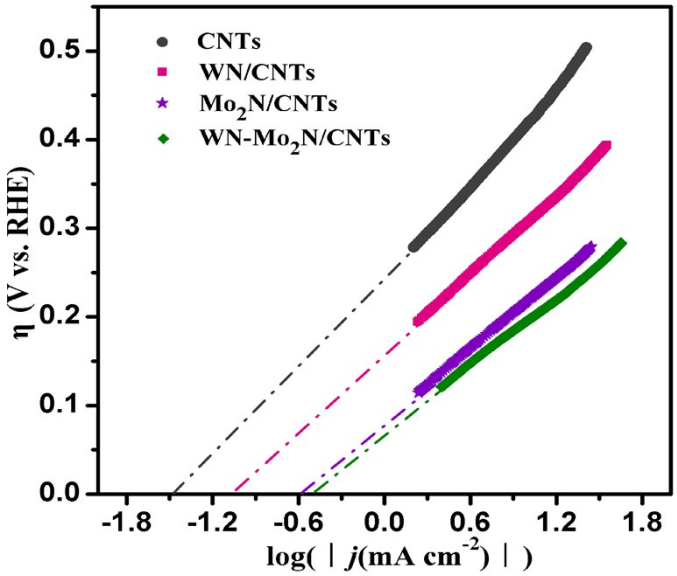

Figure S13. The curves of exchange current density of CNTs, WN/CNTs-50, Mo_2N/CNTs-50 and WN-Mo_2N/CNTs-50.

The exchange current density (j0) was calculated using extrapolation method. Based on Tafel equations, j0 for CNTs, WN/CNTs-50, Mo_2N/CNTs-50 and WN-Mo_2N/CNTs-50 are calculated to be 34, 89, 258 and 309 μA cm^{-2}, respectively.

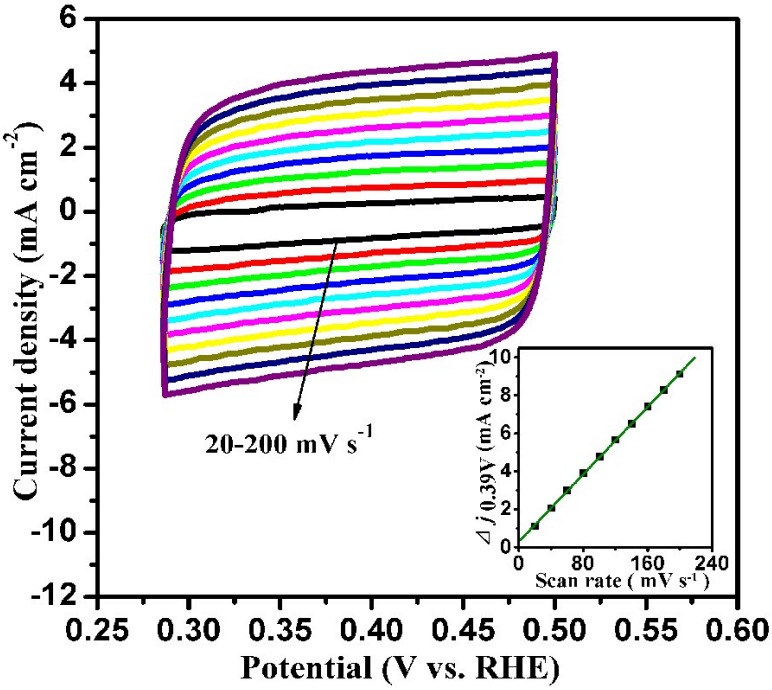

Figure S14. CVs for WN-Mo_2N/CNTs-50 with different rates from 20 to 200 mV s^{-1}. The inset is the capacitive currents at 0.39 V as a function of scan rate for WN-Mo_2N/CNTs-50 ($\Delta j_0 = j_a - j_c$). The capacitance of WN-Mo_2N/CNTs-50 is 44 mF cm^{-2}.

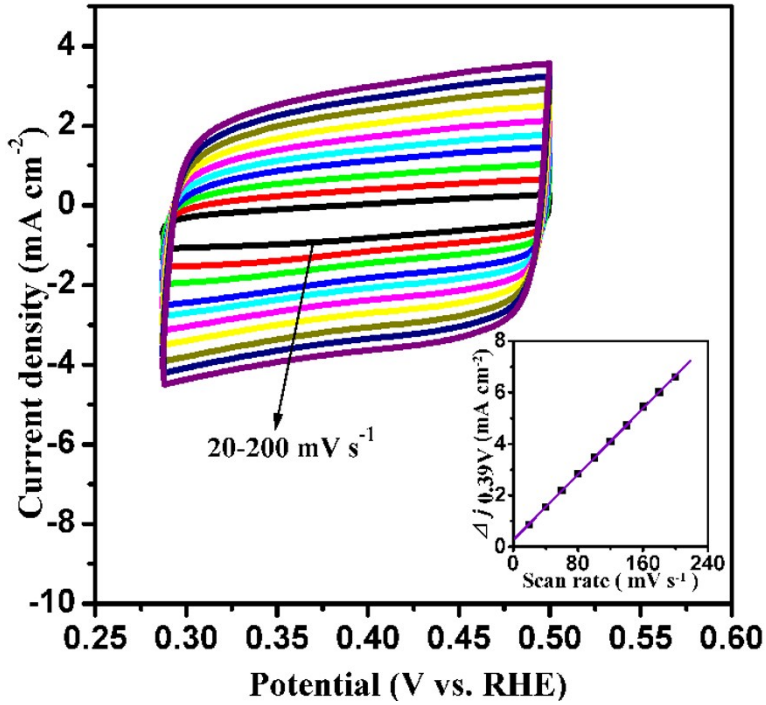

Figure S15. CVs for Mo_2N/CNTs-50 with different rates from 20 to 200 mV s^{-1}. The inset is the capacitive currents at 0.39 V as a function of scan rate for Mo_2N/CNTs-50

($\Delta j_0 = j_a - j_c$). The capacitance of Mo_2N/CNTs-50 is 32 mF cm^{-2}.

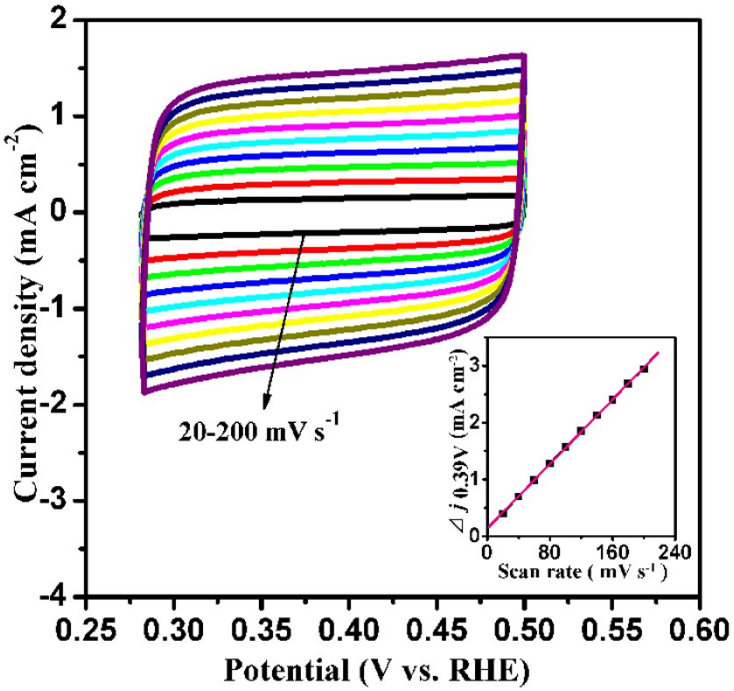

Figure S16. CVs for WN/CNTs-50 with different rates from 20 to 200 mV s^{-1}. The inset is the capacitive currents at 0.39 V as a function of scan rate for WN/CNTs-50 ($\Delta j_0 = j_a - j_c$). The capacitance of WN/CNTs-50 is 14.3 mF cm^{-2}.

The XPS of W4f in WN/CNTs, Mo3d of Mo_2N/CNTs were compared with W4f and Mo3d in WN-Mo_2N/CNTs and analyzed to identify the interaction effect of W and Mo in WN-Mo_2N/CNTs.

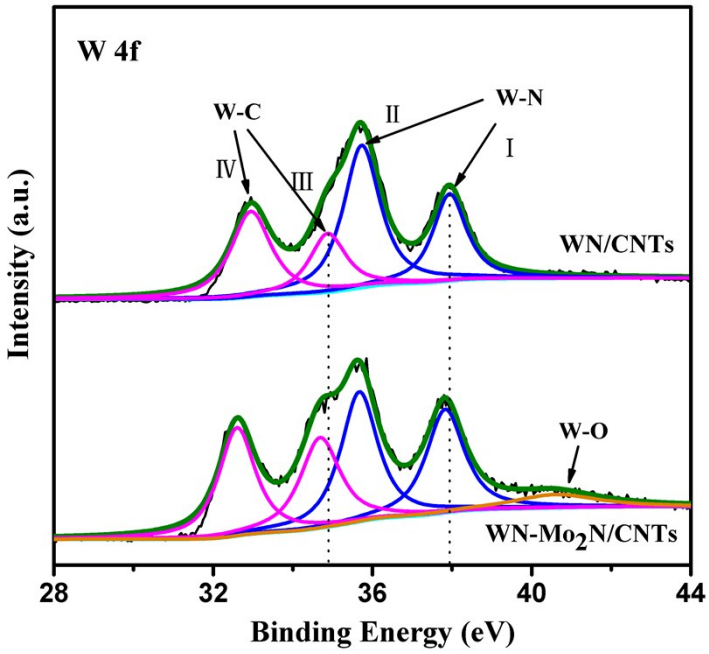

Figure S17. the W4f spectra of WN/CNTs-50 and WN-Mo_2N/CNTs-50

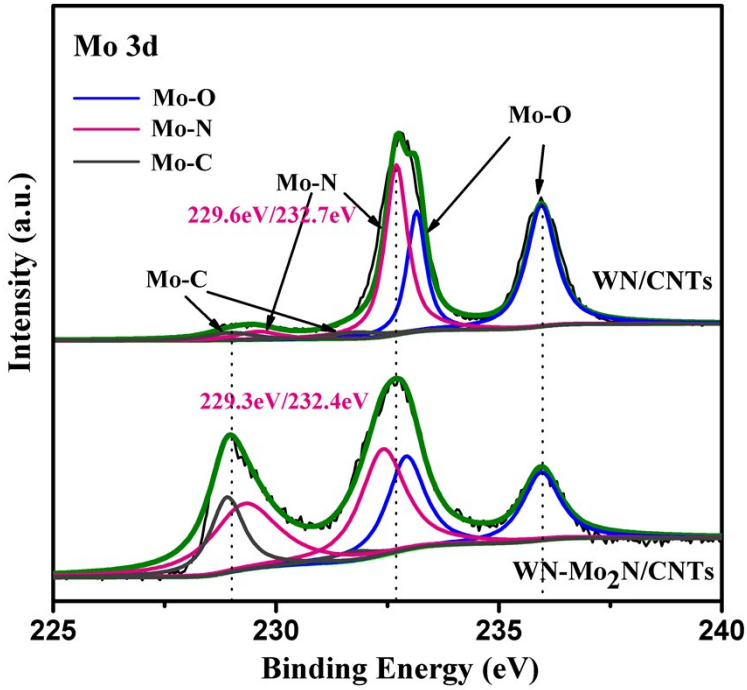

Figure S18. the Mo3d spectra of Mo_2N/CNTs-50 and WN-Mo_2N/CNTs-50.

The W4f of WN/CNTs-50 samples can be deconvoluted into two sub-groups. The peaks located at about 35.7eV and 37.9eV can be ascribed into W-N, and those located at 32.9 and 34.9 eV is due to presence of W-C. The presence of W-C should

be due the reduction role of carbon-containing species under heating.

For W4f of WN-Mo_2N/CNTs-50, after the deconvolution, the W combined with N can be observed at about 35.6 and 37.8 eV. The value has a negative shift of 0.1 eV in comparison with that of WN/CNTs-50. At the same time, the peaks relative with W-C located at 32.7 and 34.7 eV, and a negative shift of 0.2 eV can be observed. For the sample, a small peaks of W-O also emerged.

After the deconvolution, the intensive peaks of Mo-N, Mo-O with weak peak of Mo-C can be observed for Mo_2N/CNTs-50 sample. The Mo-N peaks located at 229.6 and 223.7 eV. The presence of Mo-O is due to the slight oxidation of Mo_2N surface after the exposure in air. The formation Mo-C should be due to the reaction of Mo precursor with carbon-containing gas released by A-CNTs or 1-MD.

For Mo3d of WN-Mo_2N/CNTs-50, after the deconvolution, the peaks of Mo-N, Mo-O and Mo-C can also be observed. The Mo-N peaks located at 229.3 and 223.4eV, having a shift of -0.2 eV in comparison with that of Mo_2N/CNTs. There is no obvious shift of Mo-O peaks for WN-Mo_2N/CNTs and Mo_2N/CNTs samples. Notably, the peak intensity of Mo-C peak for WN-Mo_2N/CNTs has obvious enhanced in comparison with that for Mo_2N/CNTs. The results may be due to the presence of W precursor can accelerated the reaction of Mo precursor with carbon-containing gas released by A-CNTs or 1-MD.

Based on the analysis and comparison of XPS spectra of Mo3d and W4f, we can found that the both Mo-N and W-N peaks have slight negative shift in ternary WN-Mo_2N/CNTs-50 catalyst, implying the gaining the electrons of W and Mo in WN-Mo_2N/CNTs-50. Such an enrichment of electrons should be favorable for the improvement of the HER activity. The intensive Mo-C peaks imply the enhancement of molybdenum carbide which is demonstrated to be an active catalyst for HER. So, in comparison with binary Mo_2N/CNTs-50 and WN/CNTs-50, the improvement of HER activity for ternary catalyst should be ascribed to gaining the electrons of Mo and W and enhancement of Mo-C components in ternary WN-Mo_2N/CNTs-50. Surely, the further deep analysis and understanding is essential, which should be performed in our further work.

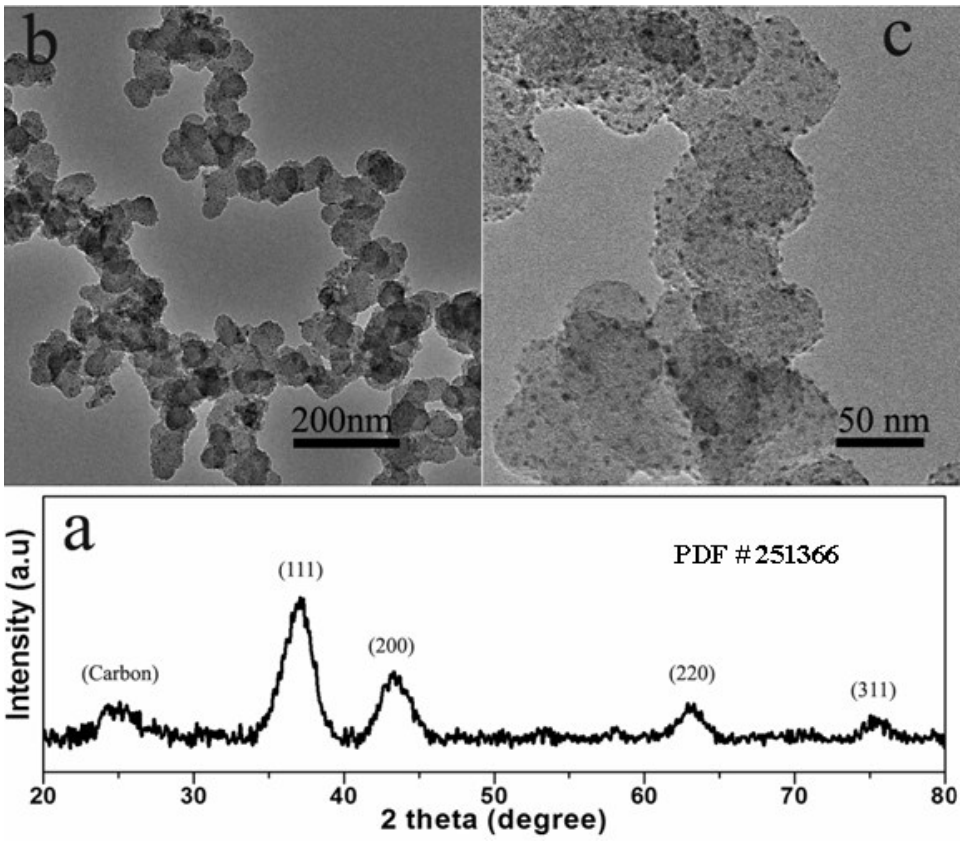

Figure S19. a) XRD and b) Large-scale TEM and c) large-magnification TEM image of Mo_2N/CB-50

In XRD pattern, a weak peak located at about 25° was characteristic for CB (Figure S19a). The broad and weak characteristics imply the poor crystalline degree of carbon. Four distinct diffraction peaks located at about 37.2°, 43.3°, 63.2°,75.6° are referred to (111), (200), (220) and (311) diffraction of primitive cubic structured Mo_2N.

The low-magnification TEM image shows the small particles were distributed well on CB (Figure S19b). The size of Mo_2N particles is about 3-4nm (Figure S19c, Figure 3c and Figure S4e). The high resolution TEM (HRTEM) images shows the spacing between two planes was 0.25 nm, corresponding to (111) crystal plane of primitive cubic Mo_2N (Figure 3d).

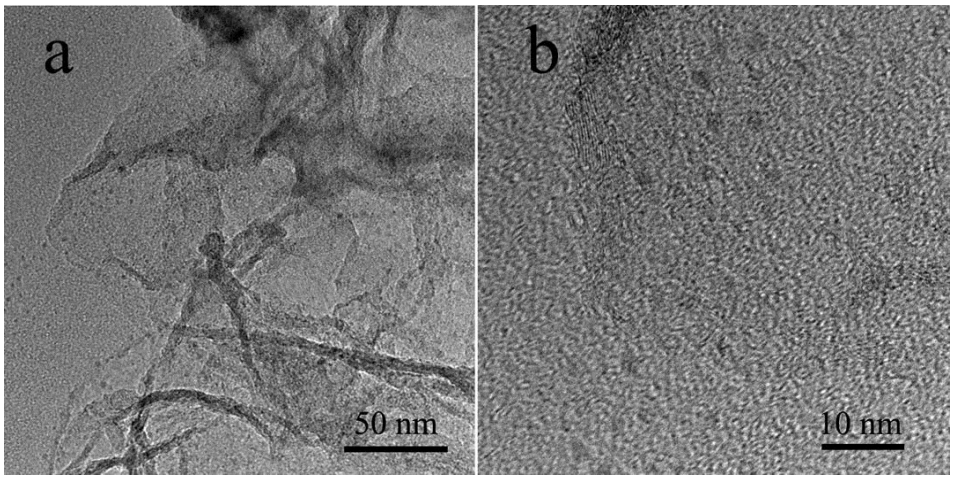

Figure S20. TEM images of WN/rGO-50

The low-magnification TEM image shows the small particles were distributed well on rGO sheets (Figure S20a). The size of WN particles is about 2nm (Figure S20b).

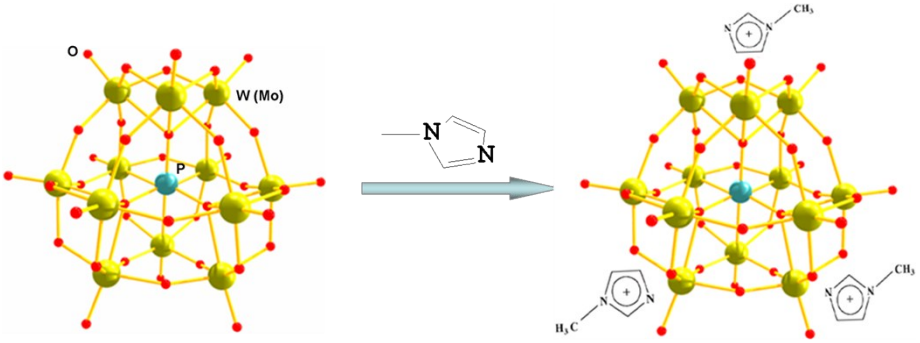

Scheme S1. the mode of binding of 1-MD to POMs. The N atoms in 1-MD can be protonized, and then coordinated with POM anions.

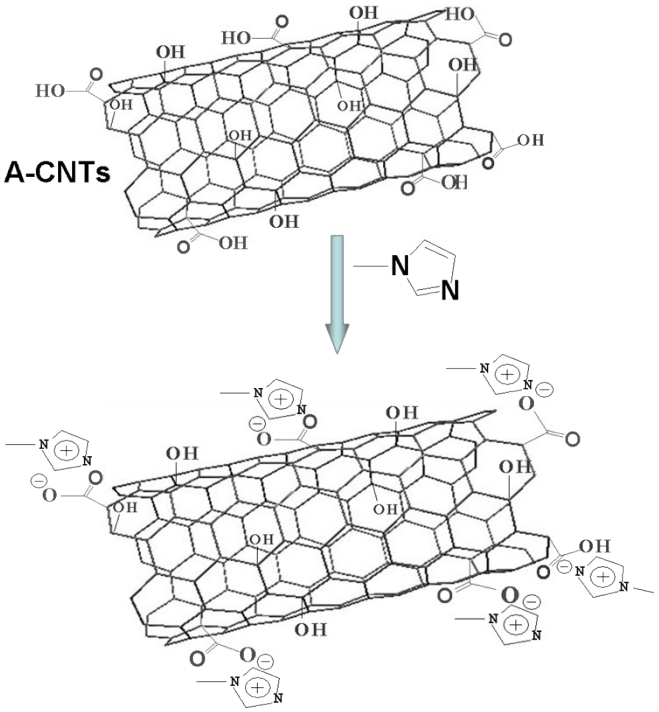

Scheme S2. the mode of binding of 1-MD to CNTs. The combination of 1-MD with CNTs should be through the electrostatic interaction or π bond.

Table S1. The summary of electrochemical performance of different catalysts.

Catalyst	η_{onset} (mV)	η at 10 mA cm^{-2} (mV)	Tafel slope (mV dec^{-1})	j_0 (μA cm^{-2})
WN/CNTs	**184**	**307**	**146**	**89**
Mo_2N/CNTs	**117**	**218**	**133**	**258**
WN-Mo_2N/CNTs	**80**	**190**	**115**	**309**
CNTs	**315**	**458**	**176**	**34**